Finite-size effects in highly ordered ultrathin FePt films

Felix Kurth,[1,2] Martin Weisheit,[1] Karin Leistner,[1] Thomas Gemming,[1] Bernhard Holzapfel,[1]
Ludwig Schultz,[1,2] and Sebastian Fähler[1,*]
[1]*IFW Dresden, P.O. Box 270116, 01171 Dresden, Germany*
[2]*Institute for Solid State Physics, Department of Physics, Dresden University of Technology, 01062 Dresden, Germany*
(Received 5 February 2010; revised manuscript received 2 August 2010; published 4 November 2010)

Granular epitaxial $L1_0$ ordered FePt films of different thickness are used to study finite size effects in this hard magnetic material. Heat absorption and material evaporation have been identified as finite size effects that strongly affect ordering. For film thickness below the absorption length heating by radiation is strongly reduced, which hinders ordering. When using equilibrium heating instead, ordering in subnanometer thick films is obtained. Furthermore preferential evaporation of Fe in comparison to Pt results in composition shifts. Since the fraction of surface to volume increases with reduced particle size, this effect limits the annealing temperature in particular for small grain sizes. The control of these finite size effects allows to achieve a high degree of order ($S \geq 0.95$) also in ultrathin films. In this way, a large coercivity of up to 7.3 T at room temperature is obtained in 10 nm thick films. In films with particle sizes down to a few nanometer high $L1_0$ order is proven by a similar coercivity at low temperature, where thermal fluctuations are negligible. These films are superparamagnetic above a blocking temperature of 160 K. These highly ordered and textured nanostructures present an ideal model system to study superparamagnetism.

DOI: 10.1103/PhysRevB.82.184404 PACS number(s): 75.70.−i, 75.50.Vv, 75.60.−d, 61.46.−w

I. INTRODUCTION

$L1_0$ ordered FePt is considered a promising material candidate for future ultrahigh density perpendicular magnetic recording.[1] It fulfils the requirement of high magnetocrystalline anisotropy and at the same time high saturation magnetization. In contrast to the rare-earth-based high-performance magnets, it is also very corrosion resistant. Thus, FePt is in particular interesting for a nanoscaled microstructure exhibiting a high fraction of surface. These advantages motivated a revival of this hard magnetic material known since the 1930s (Ref. 2) and resulted in an intense research on thin films[3,4] and FePt surface alloys,[5] thick films,[6] nanoparticles prepared with chemical methods[7] and from the gas phase[8] as well as exchange coupled bulk magnets.[9]

Despite these advantages, it is still open how the key requirements for magnetic data storage can be obtained for FePt all at once: (1) a grain size of only a few nanometers to reach a high-storage density, (2) a high magnetocrystalline anisotropy which allows remanent magnetization to withstand thermal fluctuations, and (3) a high degree of texture aligning most of the magnetization along one direction. As today's (and future) recording media is based on perpendicular recording, the easy magnetization axis should be aligned perpendicular to the substrate.

Epitaxial growth on heated substrates appears to be the approach most promising to fulfill these requirements. Here we ignore all other technical issues of magnetic recording media (price, low processing temperature, short distance between grains, high uniformity of grain size, switchability by a recording head) but focus on the fundamental aspects arising when the size of the FePt particles is reduced. According to Koksharov,[10] finite size effects are defined as follows: "in the view of condensed matter physics, finite size effects are originated by the cut off of characteristic length, resulting from the geometric limitation of the particle. In certain sense, surface effects can be considered as a sort of finite size effects since the surface influence is most significant in smallest nanoparticles and should vanish for large particles."

This work is preceded by extensive work on epitaxial FePt films grown by various techniques, such as sputtering,[3,11,12] pulsed laser deposition (PLD) (Ref. 13) and molecular beam epitaxy.[14] Two different routes to obtain epitaxial growth are reported. Granular FePt films with the easy axis oriented perpendicular to the film plane can be prepared by epitaxial growth on MgO(001) at high deposition temperatures.[3,13] These films present a model system to investigate fundamental micromagnetic issues. Very high coercivities of 4.8 T,[15] 5.6 T,[13] and 7.0 T (Ref. 3) have been achieved in these particulate films due to the well-decoupled microstructure where each grain switches individually by coherent rotation.[3,4] With this, FePt is the material in which the closest approach of coercivity to the anisotropy field [11.7 T (Ref. 16)] has been achieved. In these films a well-defined microstructure of highly ordered and decoupled particles is present. This allows a discussion of magnetization behavior with regard to the Stoner-Wohlfarth model.[17] While these granular films require high deposition temperatures ($\geq$600 °C), in an alternate approach continuous epitaxial films can be grown at moderate temperatures ($\leq$500 °C) (Ref. 18) on a combined Cr/Pt buffer.[19] Such ultrathin continuous FePt and FePd films allowed an experimental examination of the electronic origin of magnetocrystalline anisotropy.[20] In continuous or coalesced films,[21] coercivities are usually lower, as reverse domains that nucleate at defects can easily move throughout the whole film.

For the present work we selected epitaxial growth of FePt(001) granular films on heated MgO(100) substrates. On films with a nominal thickness in the range from 0.5 to 10 nm, finite size effects are examined beyond the well-known superparamagnetic effect. The influence of deposition temperature, postannealing time and decreasing particle size on ordering, microstructure, coercivity, and magnetization

process is analyzed with respect to the finite size. We address mechanisms such as evaporation and optical absorption and report how this affects ordering at small particle size. The aspects are discussed with regard to ultrathin sputtered FePt particulate films,[22] where a lower degree of order was attributed to the dominance of interface energy at reduced size.

II. EXPERIMENTAL

FePt thin films were prepared on heated single crystalline MgO(100) substrates by PLD. Details on the process are described elsewhere.[23] In the present study, an Fe-Pt alloy target is used. In comparison to pure elemental Fe and Pt targets, droplet formation[24] can be avoided and a better reproducability of stoichiometry is obtained. The deposition rate per pulse was measured by a quartz microbalance before deposition and used to calculate the nominal film thickness.

Films were deposited at different temperatures. The deposition temperatures were measured by a thermocouple mounted in the ceramic heater used for radiation heating. After deposition, the films stayed on the holder in the PLD chamber and temperature was held constant for a postannealing procedure during which an additional heat reflector was moved in front of the substrate. The deposition/postannealing temperatures were varied between room temperature and 1100 °C and postannealing times up to 1 h were studied.

Structure characterization was done by x-ray diffraction (XRD) with Co K_α radiation in Bragg-Brentano geometry in a Philips X-Pert PW 3376/00 diffractometer. We determined the chemical order parameter S of the $L1_0$ phase as described in Ref. 16. The integrated intensity of an (hkl) diffraction peak, $I(hkl)$, is related to the structure factor, $F(hkl)$, by

$$I(hkl) = C_0 F(hkl)^2 LPA e^{-2M} \tag{1}$$

where C_0 is a constant, A is the illuminated area, L is the Lorentz factor, P is the polarization factor and $2M$ is the Debye-Waller factor. For $L1_0$ films the $F(hkl)$ are

$$F = 4(x_A f_A + x_B f_B) \tag{2}$$

for the fundamental peaks and

$$F = 2S(f_A - f_B) \tag{3}$$

for superlattice peaks, where $f_A(f_B)$ is the atomic form factor and $x_A(x_B)$ is the atom fraction of chemical species A (B). For our films, S is calculated from the integrated intensities of the $L1_0(001)$ superlattice and the $L1_0(002)$ fundamental peak using Eqs. (1)–(3) and calculated values for P, L, $2M$ and the atomic form factors for Fe and Pt for the two reflexes.[16,25] For $Fe_{50}Pt_{50}$ and the wavelength of 0.179 nm, this leads to the relationship $S = \sqrt{0.75 \cdot \frac{I(001)}{I(002)}}$.

For microstructure analysis, transmission electron microscopy (TEM) was carried out in a FEI Tecnai F30 in conventional TEM operation mode. Magnetic measurements were performed using a vibrating sample magnetometer inset in a Quantum Design Physical Property Measurement System (PPMS) 6100 with a maximum magnetic field of 9 T. Hysteresis loops were measured for the field applied along in- and out-of-plane directions and at temperatures between 10 and 400 K.

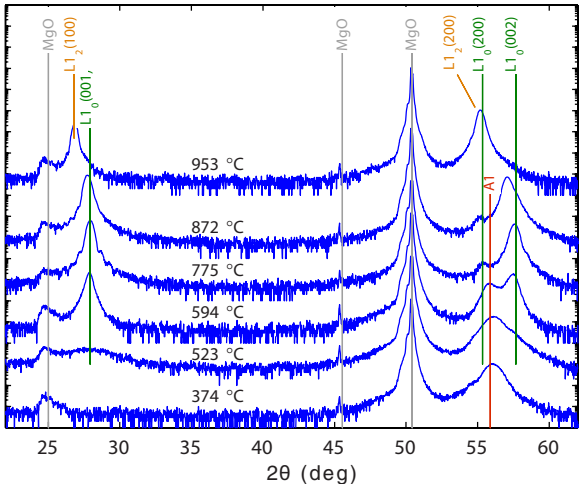

FIG. 1. (Color online) XRD patterns of FePt thin films with a nominal thickness of 10 nm deposited and postannealed for 600 s at different temperatures. The positions of bulk FePt $L1_0$, $FePt_3$ $L1_2$, and FePt A1 phase, and MgO substrate reflections are marked.

III. STRUCTURE AND ORDERING

At first, the deposition temperature dependence of $L1_0$ ordering of 10 nm thick FePt films is investigated. The postannealing time after deposition is fixed at 600 s. The XRD patterns for temperatures from 374 °C to 953 °C are shown in Fig. 1. Up to a deposition temperature of 374 °C only the (200) peak of the disordered FePt A1 phase is visible besides the substrate peaks. Increasing the deposition temperature to 523 °C leads to a slight shift of this FePt A1 peak toward the peak position of the $L1_0(002)$ peak. An increased intensity is found at the positions of the $L1_0(001)$ and $L1_0(002)$ peaks, indicating that a minor fraction of ordered $L1_0$ phase is present in addition to the A1 phase. At a deposition temperature of 594 °C, significant $L1_0$ ordering is observed. There, the $L1_0(001)$ and (002) peaks appear in addition to the A1 peak, showing a phase mixture of A1 and $L1_0$ phase. As the peaks of both phases are observed simultaneously, it can be concluded that the A1 phase transforms into the $L1_0$ phase by nucleation and growth of ordered domains, corresponding to a first order phase transition. Since in bulk $L1_0$ ordering is a first-order transition[26] as well, there is no indication that the ordering process is affected by finite size effects at this film thickness.

At 775 °C the A1 peak has vanished and only $L1_0$ peaks are observed in the XRD diagram. This shows that $L1_0$ ordering has proceeded further resulting in a highly ordered, almost single phase $L1_0$ FePt film. The $L1_0(001)$ and $L1_0(002)$ peaks dominate over the $L1_0(200)$ peak, showing the intended perpendicular alignment of the c axis. Increasing the temperature further to 872 °C leads to a shift of the $L1_0(200)$ and $L1_0(001)$ peak positions toward lower diffraction angles. At a deposition temperature of 953 °C, the $L1_0$ peaks have vanished and instead the $L1_2(200)$ and $L1_2(100)$ peaks of the $FePt_3$ phase occur. The existence of the ordered $FePt_3$ $L1_2$ phase instead of the FePt $L1_0$ phase is not expected for a $Fe_{50}Pt_{50}$ composition. This suggests the occurrence of a composition shift, which is discussed in Sec. VI.

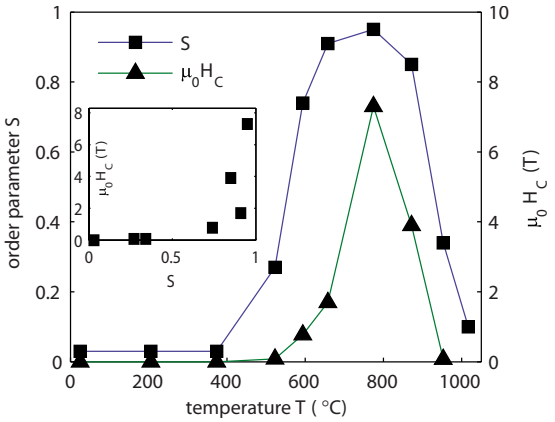

FIG. 2. (Color online) Order parameter S (squares) and coercivity H_C (triangles) of FePt thin films with a nominal thickness of 10 nm deposited and postannealed for 600 s at different temperatures.

The order parameter S for the $L1_0$ phase calculated from of the XRD patterns is summarized in Fig. 2. Ordering starts around 550 °C. The strong nonlinear increase in S for higher temperatures up to $S=0.95$ at 775 °C is due to the exponentially increasing diffusion length. S reaches its maximum value of 0.95 at the deposition temperature of 775 °C. The results agree with those of Shima *et al.*[3] who achieved an order parameter of 0.95 at 780 °C in granular FePt films. In the present experiments, a further increase in temperature leads to a rapid decrease in S due to the formation of the $FePt_3$ $L1_2$ phase.

Casoli *et al.*[27] showed that a postannealing procedure can improve ordering. Hence, for the deposition temperature of 775 °C, where the highest degree of $L1_0$ order is achieved, the postannealing time dependence of ordering is studied. Figure 3 shows that at $t=0$, an ordering parameter of $S=0.87$ is obtained. The short time of about 120 s required to deposit 10 nm is thus not sufficient for complete ordering. This holds especially for the top of the film that experienced the least time at high temperature. When the postannealing procedure using the reflector is applied, S increases to $S=0.95$ for $t=600$ s and then remains almost constant for longer annealing times.

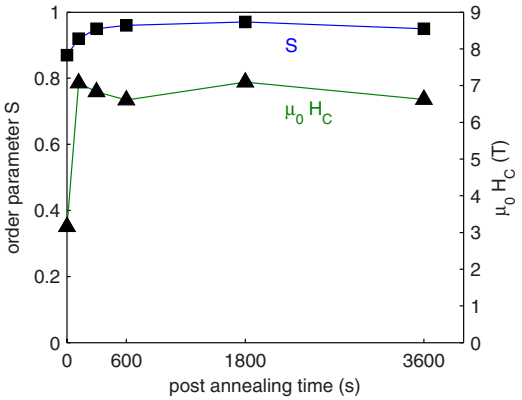

FIG. 3. (Color online) Order parameter S (squares) and coercivity H_C (triangles) of FePt thin films with a nominal thickness of 10 nm deposited and postannealed at 775 °C for different postannealing times.

At this point it is interesting to compare the optimum conditions obtained here (≈800 °C, 600 s) with previously published time-temperature-transition (TTT) diagrams for ordering.[28,29] The diagrams of Barmak *et al.*,[28] based on thermodynamic calculations, typically give shorter times in the milliseconds range to achieve up to 95% ordering. In contrast, the summary of Buschbeck *et al.*,[29] evaluating experimental XRD and magnetic data, gives a longer time scale for ordering in the range of s to min, which is comparable to the results of the present study. This suggests that for experiments, additional microstructural factors not considered in the calculations (size and number of ordered domains and antiphase boundaries) slow down the ordering process. Both calculated and measured TTT diagrams point out an optimum temperature of around 800 °C and above. The strong decrease in order at higher temperatures observed in the present experiments is not expected, as also these higher temperatures are still well below the thermodynamic ordering temperature of 1300 °C—an aspect discussed later in detail.

IV. MORPHOLOGY

It is well known that FePt films grow in a granular fashion on heated MgO substrates and coalescence is observed at relatively high thickness.[30] The nominal thickness range up to 20 nm in the present study is well below the critical nominal thickness of 50 nm reported by Li *et al.*[30] for the transition from granular to coalesced state. The granular morphology results in an infinite electrical resistivity, which is measured for all films with a nominal thickness of 10 nm produced at temperatures higher than 374 °C. For these granular films, the height of the individual particles is expected to deviate from the nominal thickness.

For smooth thin films the interference of x-rays reflected from a finite thickness results in so-called satellite reflections in the neighborhood of crystal reflections. Their position can be used to determine the film thickness h with the high accuracy of XRD. h is determined from the position shift using

$$h = \frac{n\lambda}{2\,\sin(\Theta_{peak} - \Theta_{satellite})},$$

where n is the order of the satellite peak, λ is the wavelength and Θ is the peak position. Here, satellite reflections are also observed for granular films deposited at 775 °C (Fig. 4). The existence of satellite reflections indicates a very homogeneous island height as a thickness variation would smear these out. As expected for the granular films, the particle height is noticeably higher than the nominal thickness of 10 nm. From the TEM cross-sectional image a particle thickness of 15 nm is observed for the film annealed for 600 s [Fig. 5(a)], agreeing with the XRD evaluation (Fig. 4). The parallel interfaces of the particles that result in the satellite reflections are clearly visible in the TEM micrographs. For this film, an average lateral grain diameter of 45 nm is found from an evaluation of scanning electron microscope top views (not shown). The particles can be described as flat rectangles with rounded corners.

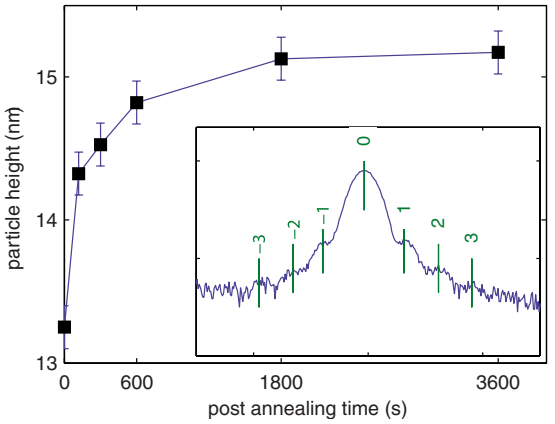

FIG. 4. (Color online) Particle height of films with a nominal thickness of 10 nm deposited and postannealed at 775 °C in dependence of the postannealing time. The inset exemplarily shows a magnified $L1_0$-(001) peak from Fig. 1 (775 °C, 600 s) with marked satellite peaks that were used to determine the particle height.

The mean particle height, as determined by the satellite reflections, increases from 13 nm ($t=0$) to 15 nm with prolonged postannealing time, indicating coarsening of the microstructure. Compared to the chemical ordering, which is almost completed after 300 s (see Fig. 3), the changes in microstructure occur during considerably longer time. This suggests that diffusion of atoms (possibly also at the surface) allows to increase h and thereby minimize the surface energy of the particles. This effect is even more pronounced for a smaller nominal thickness of 1 nm, as shown in Figs. 5(b) and 5(c). These small particles exhibit a shape close to half

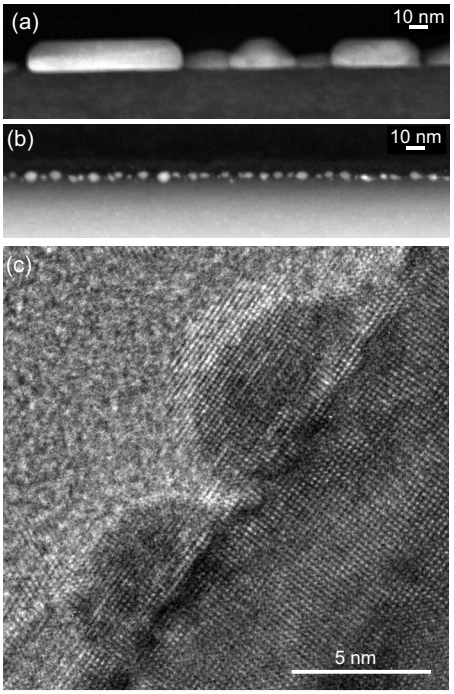

FIG. 5. TEM cross-sectional images of granular FePt films deposited and postannealed at 775 °C for 600 s with a nominal thickness of (a) 10 nm and (b) 1 nm. (c) is a higher resolution TEM cross-sectional image of the film with a nominal thickness of 1 nm.

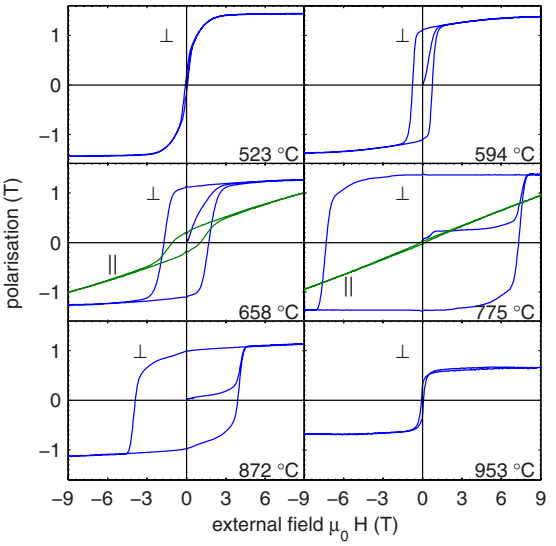

FIG. 6. (Color online) Out-of-plane (⊥) and in-plane (∥) hysteresis loops of FePt thin films with a nominal thickness of 10 nm deposited and postannealed for 600 s at different temperatures.

spheres with a minimized surface area. The particle diameter is around or below 5 nm and thus significantly smaller compared to the nominally 10 nm thick film.

V. MAGNETIC PROPERTIES

A. Highly coercive films

For annealing temperatures between 523 °C and 953 °C and an annealing time of 600 s, the out-of-plane magnetic hysteresis loops are displayed in Fig. 6. Up to 523 °C coercivity is very low. Coercivity increases for higher annealing temperatures and reaches a maximum value of 7.3 T at 775 °C. The saturation polarization is 1.4(3)T for annealing temperatures up to 775 °C, which agrees within the accuracy of these measurements with the expected value for FePt.[31]

For 658 °C and 775 °C, the in-plane curves are added in Fig. 6. When depositing the film at 658 °C the in-plane curve is mostly closed. However, there is still some remanence present, which indicates that part of the material has its easy axis aligned in-plane. This agrees with the XRD intensity of the $L1_0$ (200) reflection still being observed at this deposition temperature. When increasing the deposition temperature to 775 °C, the in-plane hysteresis is completely closed and exhibits a low slope which indicates a rotation of magnetization along a hard axis. In agreement with the texture measured by XRD this confirms the nearly perfect perpendicular alignment of the easy axis. This allows to use the extrapolation of the hard and easy axis curves to determine their intersection as the anisotropy field. The anisotropy field is about 12 T, which is expected for highly ordered $L1_0$ FePt.[16]

When annealing at temperatures above 775 °C, both coercivity and saturation polarization are reduced. This can be explained by a partial formation of the $FePt_3$ phase, as has been suggested by the XRD diagrams. The antiferromagnetic $FePt_3$ $L1_2$ structure has a Néel temperature of 160 K.[32] At

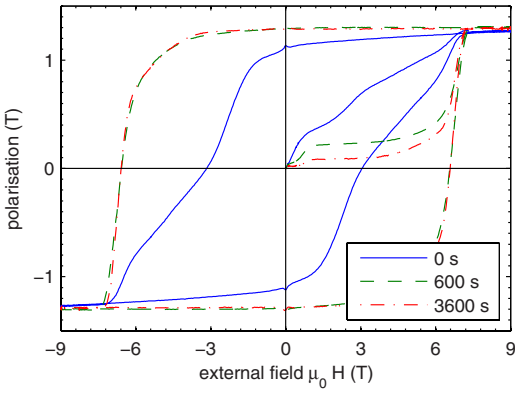

FIG. 7. (Color online) Out-of-plane hysteresis loops of FePt thin films with a nominal thickness of 10 nm deposited and postannealed at 775 °C for annealing times of 0, 600, and 3600 s.

room temperature the behavior should be paramagnetic, leading to the observed decrease in the saturation polarization.

In Fig. 7 the out-of-plane magnetization curves for annealing times of 0, 600, and 3600 s are plotted. A coercivity of 3.1 T is reached directly after deposition (t_A=0). The initial magnetization curve shows a step at low fields. If postannealing is applied, the coercivity is between 6.6 and 7.3 T, almost independent of the annealing time (see also Fig. 3). However, an increased annealing time leads to a flattening of the virgin curve. The step at low applied fields is reduced and a strong increase in magnetization leading to saturation only occurs at field strengths close to coercivity. This behavior can be explained by the domain state of the particles. For small single domain particles, the magnetization process is dominated by rotation of magnetization. In this case initial magnetization curves show a slow increase in magnetization with applied field. For larger multidomain particles, initial magnetization increases steeply by domain wall movement and saturates easily.[33] The critical diameters for the formation of single domain particles in granular FePt films are reported to be approximately 180 nm for a nominal thickness of 20 nm (Ref. 30) and 55 nm for a nominal thickness of 10 nm.[34] Since for the film with a nominal thickness of 10 nm a particle diameter of 45 nm is found in our study, the majority of all particles will be in single domain state. However, as the particle diameters follow a lognormal distribution (not shown here), a certain number of multidomain particles will be present in the film. Directly after deposition, the initial magnetization curve (Fig. 7) reflects the sum of both types of magnetization behavior: nucleation-type and rotation type. This agrees with studies of Shima *et al.*[3] that found a mixture of single domain and multidomain particles in an intermediate nominal thickness region between 5 and 25 nm. The change in the initial magnetization curve (Fig. 7) suggests that a decrease in the number of large multidomain particles is achieved by annealing. This can be explained by the increase in particle height (see Fig. 4) as the critical diameter for single domain particles is dependent on the aspect ratio. For textured, highly anisotropic FePt particles with flat ellipsoidal shape, calculations and experiments by Li *et al.*[30] revealed that the demagnetizing factor decreases when the ratio

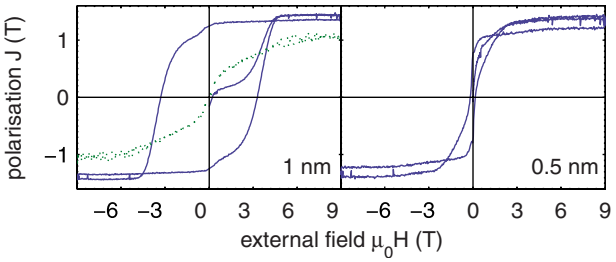

FIG. 8. (Color online) Room-temperature out-of-plane hysteresis loops of FePt thin films with nominal thickness of 1 and 0.5 nm deposited and postannealed at 775 °C for an annealing time of 600 s. For the 1 nm thick film, the in-plane curve is added as a dotted line.

of height/diameter is increased. This explains the stabilization of the single domain state in particles with greater height.

The dependency of out-of-plane coercivity on the annealing temperature and on the achieved degree of order is shown in Fig. 2 and the inset in this figure, respectively. The precondition for a high coercivity is a high magnetocrystalline anisotropy, which is strongly dependent on the degree of order in FePt. This is reflected in the presented results, where coercivity scales with the order parameter and the huge coercivities are obtained only for order parameters higher than 0.95. However, while S exhibits a broad maximum around a deposition temperature of 800 °C, coercivity peaks sharply at a deposition temperature of 775 °C. This suggests that nearly perfect order and thus maximum anisotropy in the ordered regions is required to approach the Stoner Wohlfarth limit. Okamoto *et al.*[35] reported on a linear dependency of H_A on S in $L1_0$ FePt films. The inset in Fig. 2 shows that the dependency of coercivity on S in our samples clearly deviates from this observation. One reason is that anisotropy is very sensitive to the phase fraction of $L1_0$ to A1 phase[36] and not only to the order parameter of the ordered phase. Especially in the samples grown at lower temperatures, the coexistence of $L1_0$ and A1 phase, as observed by XRD, allows the easy nucleation of reversed domains which significantly reduces coercivity. A similar nonlinear relationship has been reported by Takahashi *et al.*,[37] who also obtained high coercivity only at nearly perfect order. The high coercivities of up to 7.3 T are thus obtained due to the combination of a high degree of order, a granular microstructure and an almost perfect alignment of the easy axis by epitaxial growth.

B. Superparamagnetism and thermal stability

The room temperature hysteresis loops for films with a decreased nominal thickness of 1 and 0.5 nm deposited and postannealed at 775 °C are plotted in Fig. 8. For a film thickness of 1 nm, coercivity is still as high as 3.3 T. Decreasing the nominal thickness to 0.5 nm leads to a decrease in coercivity to 0.2 T.

By studying the temperature dependency of the magnetic properties, it was examined whether this low coercivity originates from superparamagnetism. In Fig. 9 the coercivity

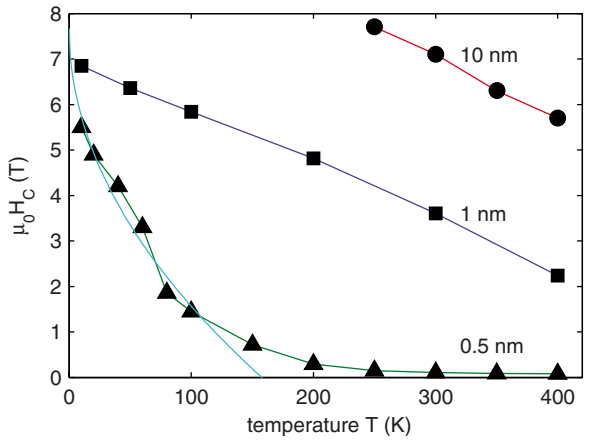

FIG. 9. (Color online) Temperature dependence of coercivity for nominal film thickness of 10, 1, and 0.5 nm. The light blue line without symbols is the fit for the 0.5 nm thickness data giving the blocking temperature and $H_C(0)$.

of films with nominal thickness of 10, 1, and 0.5 nm is plotted for temperatures between 400 and 10 K. Coercivity increases almost linearly with decreasing temperature for the 1 and 10 nm thick films. For the film with the lowest nominal thickness of 0.5 nm, the behavior is no longer linear. Selected hysteresis loops for this film at 10, 100, and 400 K are plotted in Fig. 10. At 10 K, a large coercivity value of 5.5 T is reached whereas at 400 K, coercivity has decreased to almost zero. The magnetization curve for 400 K has the shape of a Langevin function, as expected for superparamagnetic behavior. For particle sizes in the vicinity of the superparamagnetic limit, the dependence of coercivity on temperature can be described by the following function:[16] $H_C(T)=H_C(0)\{1-[\frac{T}{T_B}]^{1/2}\}$, where T_B is the blocking temperature and $H_C(0)$ the coercivity at 0 K. From a fit for the data from 10 to 100 K for the 0.5 nm thick film a T_B of 160 K and a $\mu_0 H_C(0)$ of 7.7 T $\pm$ 1.2 T is obtained (see Fig. 9).

VI. DISCUSSION

A high room-temperature coercivity of 7.3 T is achieved for 10 nm thick films, which exceeds the highest reported

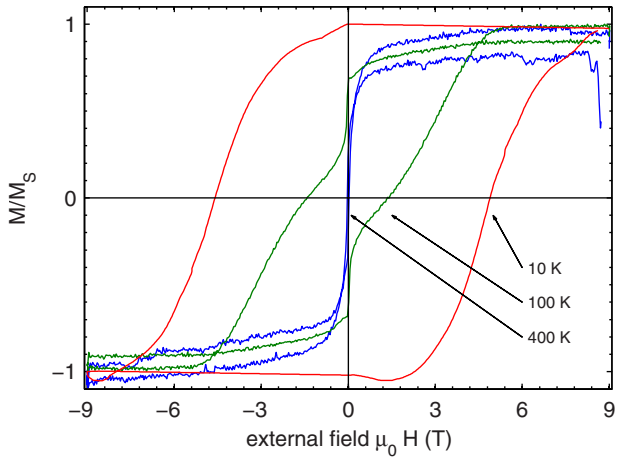

FIG. 10. (Color online) Out-of-plane hysteresis curves measured at different temperatures for a nominal film thickness of 0.5 nm.

value of 7.0 T found by Shima *et al.*[3] in FePt films. At a nominal thickness of only 0.5 nm, highly ordered films are achieved that exhibit very high coercivity at lower temperatures but are small enough to be superparamagnetic at room temperature. The superparamagnetic limit at room temperature for FePt spherical particles is expected at 3 nm,[1] which agrees with the particle size reached in the 0.5 nm thick film. Up to now, because of the difficulties encountered during the ordering of small particles, only superparamagnetic FePt particles with no or low $L1_0$ order have been reported.[8,38]

Superparamagnetism is a finite size effect. Further finite size effects had to be considered for obtaining a high degree of order required to reach a high blocking temperature in these small particles. In the following the role of heat absorption and evaporation of material at reduced sizes is analyzed. Heat absorption in the ultrathin films differs significantly from bulk samples. As the MgO substrate is transparent for infrared light, most of the heat radiation of the heater is transmitted through the substrate and then partially absorbed within the FePt film. As a rough estimate, the mean absorption length in FePt is about 15 nm from the averaged absorption coefficients of elemental Fe and Pt.[39] Thus, thin films below 10 nm absorb only a low fraction of the heat radiation. To increase the energy uptake required for ordering, in the present experiments a heat reflector was mounted during the postannealing stage in front of the substrate. With this, the samples are irradiated from both sides instead of only from the back side, which leads to a significantly increased absorbed energy in the film. As a first approximation this geometry may be considered as an oven, which allows to reach thermal equilibrium. Therefore, all size dependent changes in the optical properties may be neglected. In the present work, the heat reflector is used for all samples to eliminate the film thickness dependence of heat absorption. This allows to reach a high degree of order for film thickness below 1 nm while in our previous experiments without reflector a film thickness of 10 nm or above had been necessary.[23]

In other studies, for example, in epitaxial FePt(001) particles coated with Pt and Ag (Ref. 17) or surrounded by Al_2O_3 and SiO_2,[22] the size dependence of coercivity was explained by a hindrance of ordering when interfacial regions gain importance. Takahashi *et al.*[22] reported that FePt particles embedded in Al_2O_3 and SiO_2 do not order below a critical diameter of 4 nm. It was suggested that for such small particles, the growing influence of the interfacial energy stabilizes the A1 phase and inhibits $L1_0$ ordering. This agrees with order parameter calculations based on diffuse-interface theory predicting a critical size of 2 nm (Ref. 22) and density functional theory calculations[40] showing that multiply twinned morphologies are favored over the $L1_0$ phase for particle diameters below 3 nm. For the film with a nominal thickness of 1 nm in the present study, semispherical particles with diameters around or below 5 nm are observed. As coercivity still reaches a high value of 3.3 T and 6.9 T at room temperature and 10 K, respectively, a high degree of $L1_0$ ordered phase must be present, which is not expected for a size close to the critical size of ordering. For the thinner film of 0.5 nm nominal thickness, particle diameter is expected to be below the predicted critical size for ordering. The huge coercivity at low temperatures proves that these

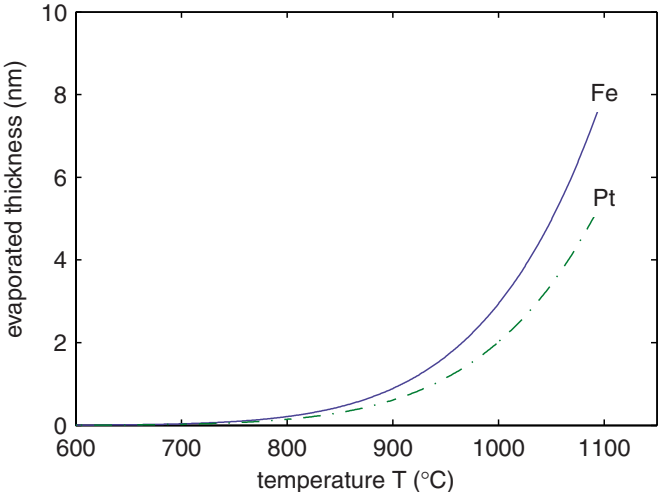

FIG. 11. (Color online) Calculated evaporated material thickness for Fe and Pt as a function of temperature during a postannealing time of 600 s.

particles are still highly ordered but superparamagnetic at room temperature. Hence these experiments demonstrate that even though the dominance of surface energy may hinder ordering at lower sizes to some extent, a consideration of the different optical properties at film thickness below 10 nm allows to achieve high order in ultrathin films. Our study shows that with this approach, ordering of FePt is possible at least down to the sizes required to increase recording density far beyond todays media.

For a high degree of order, a film preparation using the adapted heating procedure developed in this study and high deposition temperatures above 800 °C suggested by TTT diagrams[28,29] would be optimal. However, the present results reveal that at elevated temperatures preferential material evaporation can become important and affect ordering. In previous studies, deposition temperatures for epitaxial FePt thin films ranged from 200 °C (Ref. 41) to about 800 °C.[3,4] In the present study, FePt film deposition at even higher deposition temperatures up to 1017 °C has been investigated. At temperatures above 775 °C, a decreased $L1_0$ order parameter is observed and instead the $FePt_3$ phase is forming. The appearance of the $FePt_3$ phase is not possible at a $Fe_{50}Pt_{50}$ composition but requires a significant enrichment of Pt. As for all films the same amount of material arrived during deposition, this shift in film composition must be attributed to evaporation losses. The vapor pressures of Fe and Pt differ, hence the Knudsen equation can be used to estimate the evaporation thickness. In Fig. 11 the evaporated film thickness during postannealing is shown for both elemental materials[24,42] as a function of temperature. Below 775 °C evaporation losses can be neglected while at higher temperatures a significant fraction of the material can evaporate. For 960 °C, e.g., an evaporated thickness of 2.5 nm for Fe and 1.7 nm for Pt is calculated. For a 10 nm thick film, this results in a thickness decrease and at the same time stoichiometry change. This loss of iron at higher temperatures explains the observed formation of the Pt-rich $FePt_3$ $L1_2$ phase, which leads to the decreased $L1_0$ order and lower coercivity. This preferential evaporation occurs at the surface and thus gains importance when the surface to volume ratio increases significantly with reduced particle diameter. As the diffusion length of Fe in FePt (4 nm at 800 °C and 600 s) (Ref. 43) is in the range of the particle heights studied, this preferential evaporation can be considered as finite size effect. Hence, for thinner films, the optimum temperature in a TTT diagram has an upper limit by evaporation. This effect becomes more important when reducing the diameter to a few nanometer, even though part of the Fe loss may be compensated by the Pt termination at the surface.[44] This, in addition to the influence of surface energy,[22,40] may be the reason that also in our study, despite the adapted heating procedure, smaller particles do not reach the huge coercivities obtained in thicker films.

VII. CONCLUSION

In this work, granular epitaxial FePt films are used as a model system to study several finite size effects in highly anisotropic magnetic nanostructures. The influence of thickness, deposition temperature and postannealing procedure on structure, morphology and magnetic properties is analyzed. We identified the reduced absorption of heat radiation at the nanoscale as a key factor hindering ordering. Using an appropriate postannealing procedure with a radiation shield allows to compensate for the size-dependent optical properties and results in a high degree of order down to a particle size of a few nanometers.

As a second finite size effect the preferential material evaporation at the surface must be considered. Reaching a high degree of $L1_0$ order in all particles requires long annealing times at high temperature, which may result in an unfavorable deviation from stoichiometry for nanoparticles of just a few nanometers.

When considering these effects during sample preparation, highly ordered ($S \geq 0.95$), highly textured granular films with grain diameters well below 5 nm can be prepared. Large grains reach coercivities up to 7.3 T at room temperature. But ordering can also be obtained in such small grains that they exhibit coercivity up to 7 T only at very low temperatures but become superparamagnetic above 160 K. Since these samples combine a high degree of order, small grain sizes and a uniaxial texture they represent a model system with only two distinct magnetization states: spin up or spin down. Therefore, they will allow a significantly better experimental examination of superparamagnetism compared to present studies where these requirements are only partially fulfilled.

ACKNOWLEDGMENTS

Helpful discussion with C. Behler is gratefully acknowledged. Parts of this work were supported by the German Research Foundation (DFG), Grants No. FA 453/1 and No. FA 453/3.

*s.faehler@ifw-dresden.de

[1] D. Weller, A. Moser, L. Folks, M. Best, W. Lee, M. Toney, M. Schwickert, J. Thiele, and M. Doerner, IEEE Trans. Magn. **36**, 10 (2000).

[2] P. P. Ewald and C. Hermann, Strukturbericht, Akad. Verlagsgesellsch. M.B.H./Leipzig, 1937.

[3] T. Shima, K. Takanashi, Y. Takahashi, and K. Hono, Appl. Phys. Lett. **85**, 2571 (2004).

[4] M. Weisheit, L. Schultz, and S. Fähler, Thin Solid Films **515**, 3952 (2007).

[5] J. Honolka *et al.*, Phys. Rev. Lett. **102**, 067207 (2009).

[6] K. Leistner, H. Schlörb, M. Weisheit, L. Schultz, and S. Fähler, Appl. Phys. Lett. **85**, 3498 (2004).

[7] S. Sun, C. Murray, D. Weller, L. Folks, and A. Moser, Science **287**, 1989 (2000).

[8] B. Rellinghaus, S. Stappert, M. Acet, and E. F. Wassermann, J. Magn. Magn. Mater. **266**, 142 (2003).

[9] J. Lyubina, I. Opahle, K. Müller, O. Gutfleisch, M. Richter, M. Wolf, and L. Schultz, J. Phys.: Condens. Matter **17**, 4157 (2005).

[10] Y. A. Koksharov, in *Magnetic Nanoparticles*, edited by S. P. Gubin (Wiley VCH, Weinheim, 2009), Chap. 6, p. 205.

[11] C. Clavero, J. R. Skuza, J. M. Garcia-Martin, A. Cebollada, D. A. Walko, and R. A. Lukaszew, Phys. Rev. B **79**, 104436 (2009).

[12] Y. Ding, J. Chen, E. Liu, B. Lim, J. Hu, and B. Liu, Thin Solid Films **517**, 2638 (2009).

[13] M. Weisheit, L. Schultz, and S. Fähler, J. Appl. Phys. **95**, 7489 (2004).

[14] A. P. Mihai, J. P. Attané, L. Vila, C. Beigné, J. C. Pillet, and A. Marty, Appl. Phys. Lett. **94**, 122509 (2009).

[15] Y. Ide, T. Goto, K. Kikuchi, K. Watanabe, J. Onagawa, H. Yoshida, and J. Cadogan, J. Magn. Magn. Mater. **177-181**, 1245 (1998).

[16] A. Cebollada, R. F. C. Farrow, and M. F. Toney, in *Magnetic Nanostructures*, edited by H. S. Nalwa (American Scientific, Los Angeles, 2002), pp. 93–122.

[17] S. Okamoto, O. Kitakami, N. Kikuchi, T. Miyazaki, Y. Shimada, and Y. K. Takahashi, Phys. Rev. B **67**, 094422 (2003).

[18] J. P. Attané, Y. Samson, A. Marty, D. Halley, and C. Beigné, Appl. Phys. Lett. **79**, 794 (2001).

[19] Y. F. Xu, J. S. Chen, and J. P. Wang, Appl. Phys. Lett. **80**, 3325 (2002).

[20] M. Weisheit, S. Fähler, A. Marty, Y. Souche, C. Poinsignon, and D. Givord, Science **315**, 349 (2007).

[21] R. Maaß, M. Weisheit, S. Fähler, and L. Schultz, J. Appl. Phys. **100**, 073910 (2006).

[22] Y. Takahashi, T. Koyama, M. Ohnuma, T. Ohkubo, and K. Hono, J. Appl. Phys. **95**, 2690 (2004).

[23] S. Fähler *et al.*, Appl. Phys. A: Mater. Sci. Process. **79**, 1529 (2004).

[24] S. Fähler and H.-U. Krebs, Appl. Surf. Sci. **96-98**, 61 (1996).

[25] B. E. Warren, *X-Ray Diffraction* (Dover, New York, 1990).

[26] P. Haasen, *Physikalische Metallkunde* (Springer-Verlag, Berlin, Heidelberg, New York, 1994), p. 148.

[27] F. Casoli, L. Nasi, F. Albertini, S. Fabbrici, C. Bocchi, F. Germini, P. Luches, A. Rota, and S. Valeri, J. Appl. Phys. **103**, 043912 (2008).

[28] D. C. Berry and K. Barmak, J. Appl. Phys. **101**, 014905 (2007).

[29] J. Buschbeck, S. Fähler, M. Weisheit, K. Leistner, J. McCord, B. Rellinghaus, and L. Schultz, J. Appl. Phys. **100**, 123901 (2006).

[30] G. Li, H. Takahoshi, H. Ito, H. Saito, S. Ishio, T. Shima, and K. Takanashi, J. Appl. Phys. **94**, 5672 (2003).

[31] T. Klemmer, D. Hoydick, H. Okumura, B. Zhang, and W. A. Soffa, Scr. Metall. Mater. **33**, 1793 (1995).

[32] S. Maat, A. J. Kellock, D. Weller, J. E. E. Baglin, and E. Fullerton, J. Magn. Magn. Mater. **265**, 1 (2003).

[33] T. Shima, K. Takanashi, Y. Takahashi, K. Hono, G. Li, and S. Ishio, J. Appl. Phys. **99**, 033516 (2006).

[34] N. Kikuchi, S. Okamoto, and O. Kitakami, J. Appl. Phys. **103**, 07D511 (2008).

[35] S. Okamoto, N. Kikuchi, O. Kitakami, T. Miyazaki, Y. Shimada, and K. Fukamichi, Phys. Rev. B **66**, 024413 (2002).

[36] R. A. Ristau, K. Barmak, L. H. Lewis, K. R. Coffey, and J. K. Howard, J. Appl. Phys. **86**, 4527 (1999).

[37] Y. K. Takahashi, K. Hono, T. Shima, and K. Takanashi, J. Magn. Magn. Mater. **267**, 248 (2003).

[38] S. Maenosono, T. Suzuki, and S. Saita, J. Magn. Magn. Mater. **320**, L79 (2008).

[39] F. Kohlrausch, *Praktische Physik* (B.G. Teubner Verlag, Stuttgart, 1996), Vol. 3.

[40] M. E. Gruner, G. Rollmann, P. Entel, and M. Farle, Phys. Rev. Lett. **100**, 087203 (2008).

[41] M. Maret, B. Gilles, I. Guhr, B. Riedlinger, M. Albrecht, G. Schatz, and E. Beaurepaire, Nanotechnology **15**, 1590 (2004).

[42] *Metals Reference Book*, 5th ed., edited by C. J. Smithells and E. A. Brandes (Butterworth-Heinemann, London, 1976).

[43] M. Rennhofer *et al.*, Phys. Rev. B **74**, 104301 (2006).

[44] M. Weisheit, L. Schultz, and S. Fähler, J. Magn. Magn. Mater. **290-291**, 570 (2005).